

Dynamic Cooling on Contemporary Quantum Computers

Lindsay Bassman Oftelie,¹ Antonella De Pasquale,² and Michele Campisi¹

¹*NEST, Istituto Nanoscienze-CNR and Scuola Normale Superiore, I-56127 Pisa, Italy*

²*Istituto Italiano di Tecnologia, Graphene Labs, Via Morego 30, I-16163 Genova, Italy*

We study the problem of dynamic cooling whereby a target qubit is cooled at the expense of heating up $N - 1$ further identical qubits, by means of a global unitary operation. A standard back-of-the-envelope high temperature estimate establishes that the target qubit temperature can only be dynamically cooled by at most a factor of $1/\sqrt{N}$. Here, we provide the exact expression for the smallest temperature to which the target qubit can be cooled and reveal that there is a crossover from the high initial temperature regime where the scaling is in fact $1/\sqrt{N}$ to a low initial temperature regime where a much faster scaling of $1/N$ occurs. This slow $1/\sqrt{N}$ scaling, relevant for early high-temperature NMR quantum computers, is the reason dynamic cooling was dismissed as ineffectual around 20 years ago; the fact that current low-temperature quantum computers fall in the fast $1/N$ scaling regime, reinstates the appeal of dynamic cooling today. We further show that the associated work cost of cooling is exponentially more advantageous in the low temperature regime. Finally, we discuss the quantum circuit complexity and optimal implementation of dynamic cooling, and examine the effects of noise on cooling in near-term quantum computers.

I. INTRODUCTION

Quantum computers offer massive advantages over classical computers in terms of execution time and memory efficiency for a subset of problems, such as optimization and simulation [1, 2]. While various physical implementations of quantum computers are still being explored (e.g., superconducting circuits, ion traps, neutral atoms), all must fulfill a fundamental set of requirements [3]. One of these requirements is the ability to initialize the quantum bits, or qubits, into a pure, fiducial quantum state. Furthermore, pure ancillary qubits will be required for fault-tolerant quantum computers to perform quantum error correction [1, 4, 5]. The preparation of pure state qubits is therefore a key hurdle in the successful implementation of quantum computers now and in the future.

The problem of initializing a large set of qubits into a pure state was first studied in the context of generating highly polarized qubits in nuclear magnetic resonance (NMR) systems to improve signal-to-noise ratios [6–8]. Since large polarization in qubits can be obtained by cooling the qubits down to very low temperatures, scientists began to explore techniques to cool qubits below temperatures that can be achieved with direct, physical cooling methods (e.g., cooling with lasers or large magnetic fields). Schulman and Varizani were the first to propose effective cooling of qubits for quantum computation with the application of certain logic gates on the qubits [9], which following Ref. [10], we refer to as *dynamic cooling*. Their proposal, based on entropy manipulation in a closed system, cools a subset of qubits (e.g., a single target qubit) at the expense of heating the others by performing unitary operations on the entire set of qubits, see Fig. 1.

In the high temperature regime, which was relevant for the NMR-based quantum computers available at the time dynamic cooling was proposed, the Shannon bound establishes that the target qubit can be dynamically cooled at most by a factor of $1/\sqrt{N}$, where N is the total number of qubits [11, 12]. This slow scaling led to the dismissal of dynamic cooling as an impractical method for cooling qubits, and gave thrust to further research aimed at beating Shannon’s bound. Since the bound

holds for closed systems, subsequent proposals extended the scenario to open systems by allowing a subset of qubits to interact with the environment (i.e., a heat bath), thereby achieving cooling beyond Shannon’s bound [11, 12]. Such techniques are usually referred to as heat bath algorithmic cooling (sometimes simply algorithmic cooling) [13–27].

However, quantum computing technology has undergone a dramatic revolution in the last two decades, with high-temperature NMR quantum computers falling out of favor as newer models that operate at very low temperatures (e.g., superconducting circuits, ion traps) have shown great promise [28, 29]. In tandem, thanks to the development of quantum thermodynamics, much interest has grown within the scientific community in regard to the possible advantage, in terms of energy consumption, of quantum technology in general and quantum computing in particular [30].

Here, we re-examine dynamic cooling in light of the scientific and technological advancements that have been achieved since its inception over two decades ago. We consider a set of N identical qubits, each initially in thermal equilibrium at some temperature T , that undergoes dynamic cooling via a global unitary transformation U , schematically represented in Figure 1. After such a transformation, the ground and excited state populations of a target qubit change, thereby affecting a

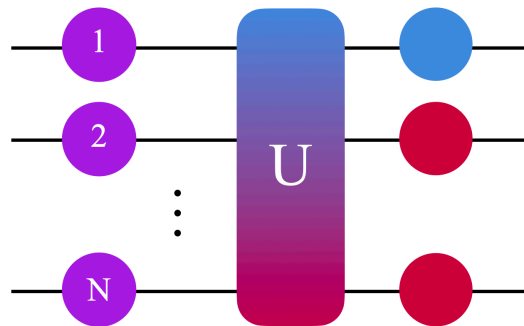


FIG. 1. Schematic of the dynamic cooling of a single target qubit amongst N identical qubits.

change in its temperature. We analytically solve the problem of finding the smallest final temperature T' that can be achieved as a function of initial temperature T , qubit resonant frequency ω , and total number of qubits N . This allows us to unveil a crossover from the expected $1/\sqrt{N}$ scaling at high T to a much faster, unexpected, $1/N$ scaling at low T .

We also provide an analytical expression for the minimal work cost associated to maximal cooling and show that it scales linearly with N (i.e., it is extensive) and displays distinct behaviours at low and high temperature. While it vanishes like $1/T$ in the high T regime, it vanishes exponentially as $e^{-1/T}$ in the low T regime.

These results evidence that dynamic cooling behaves very differently at high and low temperatures. In particular, at low T it is much more effective in terms of system-size scaling and energy cost. Since current quantum computers operate in the low T regime (unlike early NMR quantum computers), these results reinstate the appeal of dynamic cooling for generating pure state qubits for quantum computation. Given this renewed viability, we discuss the optimal implementation of dynamic cooling in terms of quantum circuits and examine the effect of noise on cooling on near-term quantum computers. Our re-examination of dynamic cooling suggest that it is a promising technique for preparing pure state qubits on near-future quantum computers once noise is reduced to low enough levels.

II. MAXIMAL COOLING

The initial state of the global system reads

$$\rho = \bigotimes_{i=1}^N \left(\frac{e^{-\beta H_i}}{Z(\beta)} \right) \quad (1)$$

where $\beta = 1/(k_B T)$, k_B is Boltzmann's constant and $Z(\beta) = \text{Tr } e^{-\beta H_i} = 2 \cosh(\beta\omega/2)$ is the partition function of any of the qubits, whose Hamiltonian $H_i = \hbar\omega\sigma_z^i/2$, is here expressed in terms of the Pauli operator σ_z^i , the reduced Plank's constant \hbar and the resonant frequency ω . All qubits are assumed to have the same resonant frequency.

Let $|i_1 i_2 \dots i_N\rangle$ denote the tensor product $|i_1\rangle_1 \otimes |i_2\rangle_2 \otimes \dots \otimes |i_N\rangle_N$ of the eigenvectors $|i_k\rangle_k$, of the operators σ_z^k , $k = 1, 2 \dots N$, where $i_k = 0$ ($i_k = 1$) denotes the ground (excited) state of qubit k . We assign qubit $k = 1$ to be the target qubit to be cooled and let $P_0 = e^{\beta\hbar\omega/2}/Z(\beta)$ and $P_1 = e^{-\beta\hbar\omega/2}/Z(\beta) = 1 - P_0$ denote the initial ground and excited state populations of the target qubit, respectively. Similarly, let $P'_0, P'_1 = 1 - P'_0$ denote the final ground and excited state populations of the target qubit after application of the cooling unitary.

To maximally cool the target qubit, the goal is to minimise P'_1 over all possible global unitaries U . This problem is equivalent to finding the set of unitaries that minimizes the expectation value of the final energy of the target qubit $u' = \hbar\omega(P'_1 - P'_0) = \hbar\omega(2P'_1 - 1)$. Thus, we must solve the minimization problem:

$$u' = \min_U \text{Tr} K U \rho U^\dagger, \quad K = H_1 \otimes \mathbf{1} \otimes \dots \otimes \mathbf{1} \quad (2)$$

where K is the target qubit Hamiltonian expressed in the Hilbert space of the total system. This problem is formally exactly the same as finding the ergotropy of a driven system (ergotropy is the maximum extractable work from a quantum system) [31]. The only difference is that solving for the ergotropy addresses the total system energy, setting K in equation 2 to the total system Hamiltonian. Here, we address the energy of a subsystem (i.e., the target qubit), using its Hamiltonian for K . Since the specific form of the Hamiltonian is irrelevant to the objective minimization problem, we may borrow techniques used to compute the ergotropy and directly apply them to our problem.

To do so, we note the critical fact that for our system, the initial state ρ commutes with the Hamiltonian K . As discussed in Ref. [31], in such a case the optimization is particularly simple: the minimum is achieved when U is a permutation matrix that maps the largest eigenstate of ρ to the smallest eigenstate of K , the second largest eigenstate of ρ to the second smallest eigenstate of K , etc. In other words, if e_i are the eigenenergies of K , then if we order the eigenvalues p_i of ρ in non-increasing fashion, that is

$$p_i \geq p_k \quad \text{for } i < k, \quad (3)$$

the minimizing unitary U in equation 2 is one that performs the permutation σ such that

$$e_{\sigma(i)} \leq e_{\sigma(k)} \quad \text{for } i < k. \quad (4)$$

In our case, the spectrum of K is highly degenerate, with only two distinct eigenvalues: $e_i = \pm\hbar\omega/2$. States of the form $|0 i_2 \dots i_N\rangle$, which are half of the total 2^N states, have an eigenenergy of K equal to $-\hbar\omega/2$, while states of the form $|1 i_2 \dots i_N\rangle$ have an eigenenergy of K equal to $+\hbar\omega/2$. Maximal cooling can thus be implemented by mapping the half of states with the highest occupation probabilities to the half of states with the lower eigenenergy $e_i = -\hbar\omega/2$. Due to the large degeneracy in the spectrum of K (as well as degeneracy in the spectrum of ρ), there will be many distinct permutations σ , and hence many distinct unitaries U , that achieve maximal cooling. Illustrative examples for $N = 3, 4$ are provided in Appendix A.

The amount of maximal cooling of the target qubit can be determined by calculating its final excited state population P'_1 . Note that P'_1 is simply the sum of the final occupation probabilities of the states $\{|1 i_2 \dots i_N\rangle\}$, which are the exact set of states to which the lowest half of probabilities are mapped. Therefore, to compute P'_1 we simply generate a list of all the occupation probabilities in non-decreasing order and sum the first half of the list.

To do so, note that the occupation probability of a state with k bits set to 0 is given by $P_0^k P_1^{N-k}$, and there will be $\binom{N}{k}$ states with this probability. States with more bits set to 0 (higher k) have higher initial occupation probabilities. Therefore, we can generate a list of the probabilities in non-decreasing order by appending the $\binom{N}{k}$ probabilities of value $P_0^k P_1^{N-k}$ to the list as we increase k from 0 to N . Summing the first half of this list will give $P'_1(P_1, N)$.

When N is odd, there are an even number of distinct values of k ranging from $k = 0$ to $k = N$. The number of probabilities for

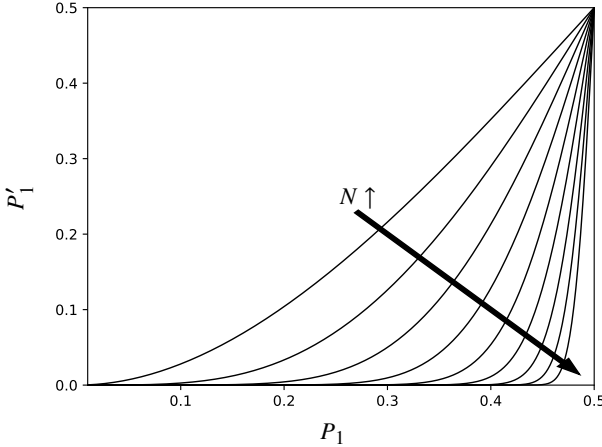


FIG. 2. Final probability of the excited state of the target qubit after maximal cooling P'_1 versus its initial probability P_1 , for increasing numbers of total system qubits N .

first half of k values ($k = 0, \dots, \lfloor N/2 \rfloor$) is equal to the number of probabilities for second half of k values ($k = \lceil N/2 \rceil, \dots, N$). Thus,

$$P'_1(P_1, N) = \sum_{0 \leq k < N/2} \binom{N}{k} (1 - P_1)^k P_1^{N-k}, \quad \text{for odd } N. \quad (5)$$

The calculation is slightly more complicated when N is even, since now, dividing the list of probabilities in half involves splitting in half the degenerate group of probabilities where $k = N/2$. This means that we must add to Eq. 5 half of the $\binom{N}{N/2}$ degenerate probabilities with value $P_0^{N/2} P_1^{N/2}$:

$$P'_1(P_1, N) = \sum_{0 \leq k < N/2} \binom{N}{k} (1 - P_1)^k P_1^{N-k} + \frac{1}{2} \binom{N}{N/2} (1 - P_1)^{N/2} P_1^{N/2}, \quad \text{for even } N. \quad (6)$$

An intriguing observation is that if we start from an odd number of qubits, adding one more qubit will not increase maximal cooling:

$$P'_1(P_1, 2s - 1) = P'_1(P_1, 2s) \quad s \in \mathbb{N} \quad (7)$$

(proof provided in Appendix B). This generalises the fact that a total of at least 3 (identical) qubits is required to obtain some cooling [32]. To see this, note that with a total of 1 qubit no cooling is possible by means of a unitary manipulation, so Eq. 7 implies that cooling with a total of 2 identical qubits is likewise impossible; a minimum of three qubits is required for dynamic cooling.

Figure 2 shows P'_1 as a function of P_1 for increasing system sizes N . Note that $P'_1(P_1, N)$ is an increasing function of P_1 , meaning that the larger the initial temperature, the larger the final temperature, which agrees with intuition. Note also that,

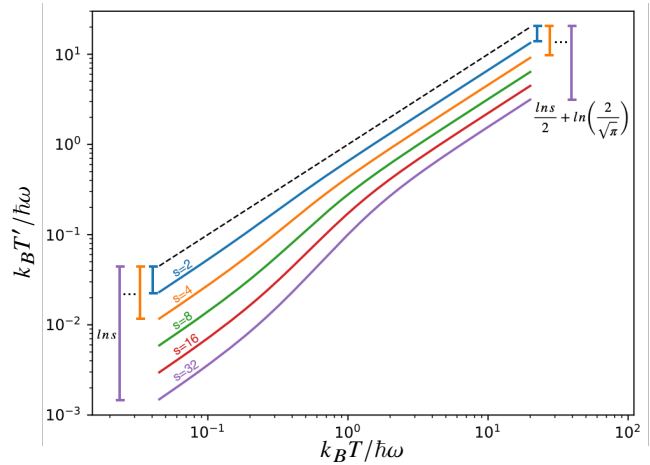


FIG. 3. Log-log plot of the minimum final temperature T' versus the initial temperature T for varying system sizes $s = \frac{N}{2}$. The black dashed line plots $T' = T$ (slope equal to 1) to guide the eye in seeing the amount of cooling that occurs. In the low temperature regime (bottom-left), plots for varying system sizes are parallel with a slope of 1, implying a linear relationship between T' and T ; and the plot for each system size s has a vertical shift of $\ln s$ from the black dashed line. In the high temperature regime (top-right), plots for varying system sizes are also parallel with a slope of 1, but now the plot for each system size s has a vertical shift of $\frac{\ln s}{2} + \ln\left(\frac{2}{\sqrt{\pi}}\right)$ from the black dashed line.

in the interval $[0, 1/2[$, $P'_1(P_1, N)$ is a decreasing function of N , namely, the larger N the higher the cooling, in agreement with what one would expect. We have

$$\lim_{N \rightarrow \infty} P'_1(P_1, N) = 0, \quad P_1 \in [0, 1/2[\quad (8)$$

meaning that as long as the initial temperature is finite and non-negative, by increasing N one can get the target qubit arbitrarily close to zero temperature. Note however the crucial fact that $P'_1(1/2, N) = 1/2$ for any N . This is because any unitary evolution leaves the completely mixed state unaltered; no cooling is possible if the initial temperature is infinite, regardless of N . This constraint is responsible for the low $1/\sqrt{N}$ scaling at high temperature, which will be discussed below.

Using the relation between the initial excited state population P_1 and temperature T , (i.e., $k_B T = \hbar\omega / \ln(1/P_1 - 1)$), as well as the analogous relation between the final, minimal excited state population P'_1 and temperature T' , we can write the final minimal temperature as

$$T' = \frac{\hbar\omega}{k_B} \frac{1}{\ln([P'_1(\frac{1}{e^{\hbar\omega/(k_B T)} + 1}, N)]^{-1} - 1)}. \quad (9)$$

Figure 3 shows a log-log plot of T' versus T for various system sizes $N = 2s$. The black dashed line plots $T' = T$ to guide the eye in seeing the amount of cooling that occurs. In both the small and large temperature regimes, there is a linear relationship between T' and T (the slope of the log-log plots is 1) but the coefficient of proportionality (i.e. the vertical shift of the plots) scales differently with s in the two regimes.

In the high temperature regime, P_1 is close to 1/2, hence we Taylor expand $P'_1(P_1, 2s - 1) = P'_1(P_1, 2s)$ around $P_1 = 1/2$ to obtain

$$P'_1 = 1/2 + c_s(P_1 - 1/2) + O[(P_1 - 1/2)^2] \quad (10)$$

$$c_s = 2^{2-2s} \sum_{k=0}^{s-1} \binom{2s-1}{k} (2s-2k+1). \quad (11)$$

Expanding the expression $e^{\beta\hbar\omega} = (1 - P_1)/P_1$ to first order around $P_1 - 1/2$, we obtain $\beta\hbar\omega \simeq 4(1/2 - P_1)$. Similarly, for the inverse final temperature, we have $\beta'\hbar\omega \simeq 4(1/2 - P'_1) \simeq c_s 4(1/2 - P_1) \simeq c_s \beta\hbar\omega$, or $T' \simeq T/c_s$. This explains the linear relationship between T' and T . It can be proven that $c_s = 2^{2-2s} s \binom{2s-1}{s}$, then, using Stirling's approximation, $N! \simeq \sqrt{2\pi N} (N/e)^N$, one finds that $c_s \simeq (2/\sqrt{\pi})\sqrt{s}$ in the large s limit (see Appendix C). Therefore:

$$T' \simeq \frac{\sqrt{\pi}}{2} \frac{T}{\sqrt{s}} = \sqrt{\frac{\pi}{2}} \frac{T}{\sqrt{N}} \quad \text{for } k_B T \gg \hbar\omega. \quad (12)$$

Note that $T' > T/\sqrt{N}$ because $\sqrt{\pi/2} > 1$, which means that Shannon's bound is obeyed as expected, but not saturated. Finding that the scaling $1/\sqrt{N}$ is realized in the high T regime (as opposed to just a theoretical bounding limit) is per se a non trivial result. This slow scaling is clearly visible in the top right corner of Figure 3.

In the low T regime, we have $P_1 \ll 1$. Taylor expansion of $P'_1(P_1, 2s - 1) = P'_1(P_1, 2s)$ around $P_1 = 0$ gives

$$P'_1 = a_s P_1^s + O(P_1^{s+1}), \quad a_s = \binom{2s-1}{s} \quad (13)$$

For small P_1 , we have $e^{-\beta\hbar\omega} = P_1/(1 - P_1) \simeq P_1$, and a small P'_1 . Therefore, $e^{-\beta'\hbar\omega} = P'_1/(1 - P'_1) \simeq P'_1 \simeq a_s P_1^s = e^{-s\beta\hbar\omega + \ln a_s}$. This implies $\hbar\omega\beta' \simeq s\hbar\omega\beta - \ln a_s$. Using Stirling approximation we obtain $a_s \simeq s \ln 4 + O(\ln s)$ (see Appendix D), hence $\hbar\omega\beta' \simeq s(\hbar\omega\beta - \ln 4)$. At low temperature (i.e., $\hbar\omega\beta \gg 1$) the term $\ln 4$ is negligible, therefore $\beta' \simeq s\beta$, or:

$$T' \simeq \frac{T}{s} = 2 \frac{T}{N} \quad \text{for } k_B T \ll \hbar\omega. \quad (14)$$

This reveals that in the low T regime, the fast $1/N$ scaling holds for optimal dynamic cooling. This fast scaling is clearly visible in the bottom left corner of Figure 3.

A characteristic value of $k_B T/\hbar\omega$ for contemporary quantum computers based on superconducting qubits, ion traps, or neutral atoms is $\simeq 0.2$, which places them within the start of the low T regime. For example, current superconducting qubit quantum computers typically operate at $\omega = 5$ GHz and $P_1 = 0.01$, which equates to an initial temperature of $T = 8.3$ mK. Given these values, we find $T' = 2.1$ mK for $s = 5$ ($N = 9, 10$), which is slightly above the scaling value of $T/s = 8.3/5$ mK = 1.66 mK. However, in accordance with our analysis above, the estimate T/s becomes better and better as N increases and/or as T decreases further.

III. MINIMAL WORK

Due to the high degeneracy of the spectrum of the K Hamiltonian, there is a great number of distinct permutations that achieve the desired ordering of eigenvectors for maximal cooling. A natural question is then, which among all these permutations have the smallest cost in terms of energy injection into the system, i.e., the work performed on the system, given by

$$W = \text{Tr} [H(U\rho U^\dagger - \rho)] \quad (15)$$

where $H = \bigotimes_i H_i$ denotes the total Hamiltonian. We recall that, since the initial state is passive, we have $W \geq 0$. When U realizes a permutation σ , Eq. 15 boils down to

$$W = \sum_i E_i (p_{\sigma(i)} - p_i) \quad (16)$$

with E_i the eigenvalues of H . Minimal work cost is thus determined by the following minimization problem:

$$\bar{W} = \min_{\sigma \in C} \sum_i E_i (p_{\sigma(i)} - p_i) \quad (17)$$

where C denotes the set of permutations that realize maximal cooling.

Solving this further minimization problem is straightforward. As described above, in order to achieve maximal cooling it is sufficient to map the half of states with the highest occupation probabilities to the set of states $\{|0 i_2 \dots i_N\rangle\}$. To achieve minimal work cost, within this set of states the highest probability should be assigned to the state with the lowest total system energy, the second highest probability should be assigned to the state with the second lowest total system energy, etc. The probabilities should also be mapped in an analogous way for the other half of states in the set $\{|1 i_2 \dots i_N\rangle\}$. This works because states with lower total system energies have higher *initial* occupation probabilities by definition. So assigning the highest *final* probability to the state with the lowest total system energy within each half-list minimizes the differences of the initial and final probabilities $p_{\sigma(i)} - p_i$ in Eq. 16, thereby minimizing work (see Appendix A for more details).

Computing the minimal value of work \bar{W} that must be invested to obtain maximal cooling is conceptually a simple task, but, in practice, it presents some challenges. Note that due to memory limitations, writing the 2^N dimensional arrays that list the energy eigenvalues E_i , and the populations $p_i, p_{\sigma(i)}$ quickly becomes an impractical task, as N increases (on desktop computer that happens already around $N \simeq 26$). We overcome this bottleneck by exploiting the large degeneracy in such arrays which allowed us to encode the relevant information into arrays whose sizes scale linearly, thereby allowing the evaluation of \bar{W} for N up to thousands.

Figure 4 shows the rescaled work \bar{W}/N as function of P_1 for various N . It appears clear from the numerics, that for $P_1 \in [0, 1/2]$ it is

$$\lim_{N \rightarrow \infty} \frac{\bar{W}(P_1, N)}{N} \doteq \bar{w}(P_1) = \frac{\hbar\omega}{2} (P_1 - 2P_1^2). \quad (18)$$

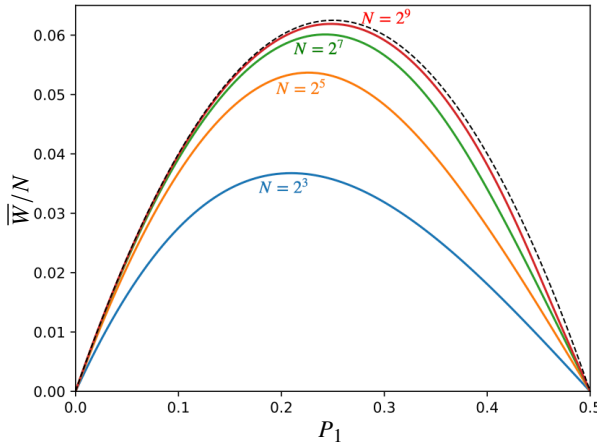


FIG. 4. Rescaled minimum work versus P_1 for various system sizes N . Dashed black line is Eq. 18.

The minimal work is extensive which evidences a trade-off between cooling power and energetic cost: The more one cools the more energy one spends. At low T , this trade-off is balanced, as the product $\bar{W}T' \sim 2\bar{w}T$ is of order 1. However, in the high T limit, the trade-off is disadvantageous because the product $\bar{W}T' \sim (\sqrt{\pi}/2)\bar{w}T\sqrt{N}$ scales like \sqrt{N} .

Note that \bar{W} goes to zero as it should for $P_1 = 1/2$ (infinite initial temperature, any U leaves ρ unaltered), and for $P_1 = 0$ (zero initial temperature, the best you can do is to leave ρ unaltered, i.e., $U = \mathbb{1}$). It is instructive to rewrite the scaling function \bar{w} in terms of initial temperature T

$$\bar{w}(T) = \frac{\hbar\omega}{2} \frac{\tanh(\frac{\hbar\omega}{2k_B T})}{e^{\hbar\omega/k_B T} + 1}, \quad (19)$$

plotted in Figure 5. In the high temperature regime \bar{w} vanishes like $1/T$ while in the low temperature regime, \bar{w} vanishes exponentially, $e^{-\hbar\omega/T}$. The inset of Figure 5 zooms in on the low temperature behaviour of \bar{w} and marks characteristic values for various contemporary quantum computers: the star represents superconducting qubits, the square represents neutral atom qubits, and the cross represents trapped ion qubits. All of them are in the low T region of the curve, while early NMR qubits are far beyond the full scale of the plot in the high T regime.

IV. IMPLEMENTATION

In order to perform dynamic cooling on quantum computers, the cooling unitary U must be translated into a quantum circuit. As stated above, there is a large family of unitaries that can achieve maximal cooling, and different quantum circuits will result from different choices of U . Near-term quantum computers are noisy, with larger circuits (in terms of number of gates) accumulating more errors than smaller ones. Therefore, from an implementation perspective, cooling unitaries that can be translated into shorter-depth circuits are more desirable.

We can compare the circuit complexities (i.e., depths) between various cooling unitaries by defining a systematic way

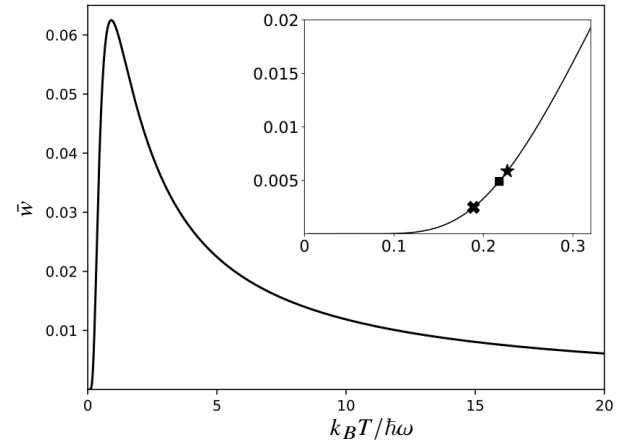


FIG. 5. Rescaled minimum work in the thermodynamic limit versus initial temperature T . Inset zooms in on exponential vanishing of work at low temperatures. Symbols denote characteristic values for various contemporary quantum computers: the star represents superconducting qubits, the square represents neutral atom qubits, and the cross represents trapped ion qubits.

to construct the quantum circuits from the particular unitary. To do this, note that every cooling unitary is defined by a set of cyclic permutations between specified states. The total quantum circuit can be constructed by building a sub-circuit for each permutation cycle and then concatenating all sub-circuits.

To describe the construction of a sub-circuit for a given permutation cycle, we focus on a swap (a cyclic permutation of length 2), and later explain how to generalize this procedure to cycles of greater lengths. Suppose we wish to construct the quantum circuit that swaps the two states defined by bitstrings b_1 and b_2 . First, we define a Gray code between the two bitstrings, which is an ordered list of bitstrings beginning with b_1 and ending with b_2 where each intermediate bitstring differs by only one bit from the previous one [33]. We define the length of the Gray code m as the number of bitstrings in the series. The length of the Gray code will be equal to one more than the number of qubits that differ between the two bitstrings (also known as the Hamming distance). Given the Gray code, a quantum circuit that implements the swap can easily be constructed using a series of k -controlled-NOT gates where $k = N-1$ and N is the number of qubits in the system. A k -controlled-NOT gate, which we denote by $C^k(X)$ is a NOT gate (i.e., a Pauli-X gate) controlled on the values of k qubits. For a swap with a Gray code of length m , the quantum circuit will contain $2m - 3 C^k(X)$ gates (see Ref. [33] and Appendix E for an illustrative example).

Constructing the sub-circuit for a cyclic permutation with a length greater than 2 is only slightly more involved. Consider, for example, the cyclic permutation of length 3: $|i_1\rangle \rightarrow |i_2\rangle \rightarrow |i_3\rangle \rightarrow |i_1\rangle$. Let the Gray code length between $|i_1\rangle \rightarrow |i_2\rangle$ be $m_{1 \rightarrow 2}$ and the Gray code length between $|i_1\rangle \rightarrow |i_3\rangle$ be $m_{1 \rightarrow 3}$. To generate the sub-circuit for this permutation, we first apply the $2m_{1 \rightarrow 2} - 3 C^k(X)$ gates to transform between bitstrings i_1 to i_2 . Next, we apply the $2m_{1 \rightarrow 3} - 3 C^k(X)$ gates to transform between bitstring i_1 to i_3 . This results in a total of $2[(m_{1 \rightarrow 2} + m_{1 \rightarrow 3}) - 3] C^k(X)$ gates. For a general permutation

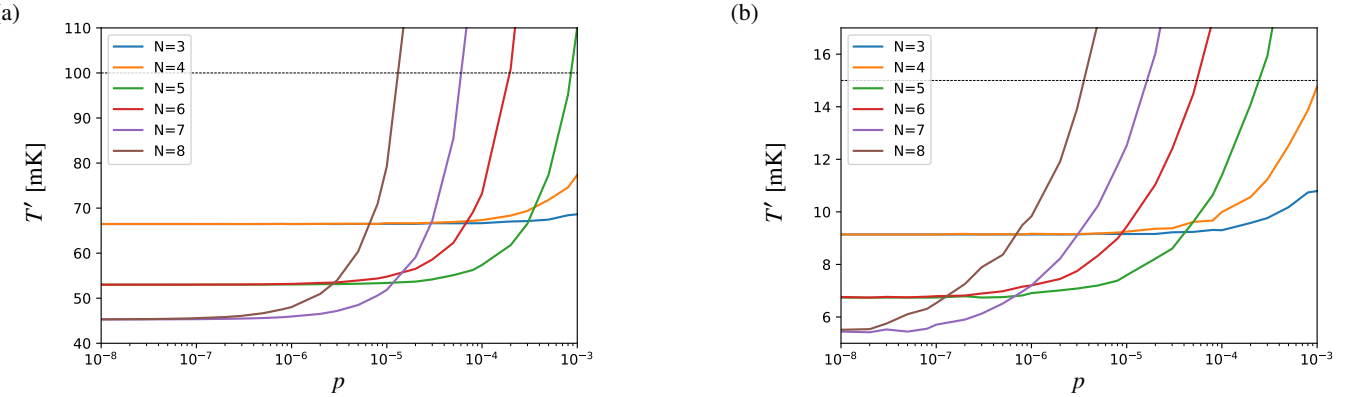


FIG. 6. Final temperatures T' of the target qubit versus noise probability p of the quantum computer for various system sizes N initialized at (a) $T = 100$ mK or (b) $T = 15$ mK. We assume a value of $\omega = 5$ GHz, which is a typical value for superconducting qubits. The black dashed lines denote initial temperatures of system. Simulation results from quantum circuits derived from the mirror protocol and executed on a noisy quantum simulator.

of length n , the total number of $C^k(X)$ gates required will be $\sum_i [2m_{1 \rightarrow i} - 3]$ where $m_{1 \rightarrow i}$ is the Gray code length from the first bitstring in the cycle to the i th bitstring in the cycle, where i goes from 2 to n .

To construct the entire circuit implementing a given cooling unitary, it is only necessary to concatenate all sub-circuits for each permutation cycle together in any order. The total circuit will therefore contain $\sum_c \sum_{i_c} [2m_{i_c} - 3] C^k(X)$ gates, where the outer sum runs over all permutation cycles c in the cooling unitary and the inner sum runs over all constituent Gray code lengths m_{i_c} of permutation cycle c .

Various protocols exist for generating maximally cooling unitaries, each of which are comprised of different sets of permutation cycles. A few protocols of interest include (i) the partner-pairing algorithm (PPA), described in Ref. [13], (ii) a minimum work protocol, which generates a unitary with minimal work cost, and (iii) a protocol we call the *mirror* protocol, in which states that have the target qubit set to 0 and have a total of $k < N/2$ bits set to 0 are swapped with their mirror image, also called the negative image (see Appendix A for more details).

The mirror protocol is, by definition, comprised of swaps between states that differ in every qubit. Therefore, the Gray code length of each swap for a system of size N will be the maximum length of $m = N + 1$. In general, the minimal work protocols contain permutations between states that do not differ in every qubit. Therefore, we expect circuits generated with the mirror protocol to be more complex than those generated with minimal work protocols. By tailoring the permutations in the cooling unitary to minimise Gray code lengths, is it possible to minimise circuit sizes. The trade-off is that designing these sets of permutations is currently a heuristic procedure, whereas the mirror protocol can easily and uniquely generate a maximally cooling permutation for each system size N .

Once the quantum circuit has been built out of $C^k(X)$ gates, it is necessary to decompose these complex, multi-qubit gates into simpler one- and two-qubit gates, which are the native gates of current quantum hardware. Ref. [34] describes how

such gates can be decomposed into a number of native gates that scales quadratically with system size N . However, if we are not concerned about relative phases between the qubits being conserved, the number of native gates can be made to scale linearly with system size N . For cooling, we are not concerned about the relative phases between qubits, rather just the populations of each state, and thus, this linearly scaling transformation technique can indeed be used.

Finally, while we have shown that increasing the total number of qubits N increases the theoretically optimal cooling capability, we note that increasing N also increases the depth of the associated quantum circuit. Therefore, for a given level of noise on a quantum computer, cooling is only possible up to some threshold N .

Figure 6 plots the final temperature of the target qubit versus the noise probability parameter p for various system sizes N for two different initial temperatures. The results are derived from quantum circuits generated using the mirror protocol to define the cooling unitary and simulated with a noisy quantum simulator (a classical computer used to simulate the performance of a noisy quantum computer). The mirror protocol was chosen because (i) it generates a unique cooling unitary for each system size N , (ii) the cooling unitary can be automatically generated with ease, and (iii) it produces more complex circuits than any other protocols, meaning that if cooling is possible with the mirror protocol, it will certainly be possible with other less complex cooling unitary. The noise model is based on a depolarizing channel [33], which can be tuned with a single noise parameter p that effectively sets the probability of error. It is implemented by inserting a randomly selected Pauli operator after each gate in the quantum circuit with probability p [35–38].

The initial temperature in each plot is indicated with a black dashed line. The colored lines indicate the final temperature of the target qubit versus the noise probability p for a range of different system sizes. Given a system with an odd number of qubits N , both plots show that adding one additional qubit (which theoretically should exhibit identical cooling capabil-

ity) impairs cooling capability at higher noise probabilities. While adding more than one qubit to the system increases cooling capability at low noise, the plots show this can actually decrease cooling capability when the noise is sufficiently high. Furthermore, for a given system size, the noise probability p at which adding a given number of qubits becomes detrimental as opposed to advantageous is smaller when the system is initialized at a lower temperature. In other words, a system initiated at a lower temperature will be more sensitive to noise on the quantum hardware. We see that in practice, there is an optimal finite number of qubits to use for dynamic cooling, which depends on the level of noise in the quantum hardware as well as the initial temperature of the qubits. We highlight that these simulations predict that cooling is possible once quantum computers obtain lower levels of noise even with circuits generated with the mirror protocol, which we expect generates more complex circuits than other protocols.

V. CONCLUSION AND OUTLOOK

In light of major developments in quantum technology, which has moved contemporary quantum computers into the low-temperature regime, we have re-examined dynamic cooling as an effective technique for cooling qubits beyond what is practically achievable with direct, physical cooling methods. We found an analytic expression for the minimum final temperature T' that can be achieved for the target qubit. We explored the high and low T regimes and discovered a crossover from a problematic scaling of $1/\sqrt{N}$ at high T to a much more efficient scaling of $1/N$ at low T . We also proposed an analytic expression for the minimal work cost \bar{W} associated to maximal dynamic cooling, which scales linearly with N . In particular, while the work cost vanishes like $1/T$ in the high T regime, it vanishes exponentially in the low T regime as $e^{-\hbar\omega/T}$.

The complexity of implementing dynamic cooling, in terms of quantum circuit size, on near-term quantum computers was also discussed. Several protocols for implementation were compared, and we suggest that protocols comprised of permutations with minimal Gray codes lengths may lead to optimal (i.e., minimal) circuit complexity. Furthermore, we simulated dynamic cooling on noisy quantum computers and found that while in theory, increasing N increases cooling capability, in practice there is a threshold N up to which cooling is possible, dependent on the level of noise on the quantum hardware and the initial temperature of the qubits.

All our results support the conclusion that in the low temperature regime, dynamic cooling is much more effective in terms of scaling and energy cost than at high temperature, and is capable of achieving cooling when noise is reduced to low enough levels. Given that current quantum computers operate in the low T regime (unlike early NMR quantum computers), these results reinstate the interest of dynamic cooling for quantum computing applications.

The biggest obstacle to the success of dynamic cooling on near-term quantum computers is the complexity of the cooling

circuit. While there is a balanced trade-off between amount of cooling and energy expenditure at low T , the complexity of the quantum circuit grows quickly with the system size N . Future work should therefore focus on finding maximally cooling unitaries (maybe with minimal work cost) with minimal quantum circuit complexity. In the meantime, one way to mitigate this is to engineer sub-optimal dynamic cooling algorithms, that is, instead of reaching the optimal final temperature (Eq. 9), we agree to reach a somewhat higher final temperature at the gain of reduced circuit complexity (Ref. [10] similarly explored sub-optimal cooling at the gain of reduced work cost).

For example, consider a system with a total of $N = n^2$ qubits, divided into n clusters, each containing n qubits. Dynamic cooling could be executed in two steps, where first, optimal cooling is performed within each of the n clusters. This will bring n qubits to $T' \simeq (2/n)T$. In the second step optimal cooling is performed among these n cooled qubits, bringing one of them to $T'' \simeq (4/n^2)T = (4/N)T$. This is less than the optimal cooling $T' \simeq (2/n^2) = (2/N)T$ but only requires unitaries acting in spaces of dimension \sqrt{N} , drastically reducing the associated circuit complexity. This algorithm can be generalised to $N = n^r$ and r steps to obtain $T^{(r)} = (2^r/N)T$. For a fixed dimension of the clusters n , and hence for a fixed circuit complexity, this amounts to cooling that scales as $T^{(r)} = N^{\frac{\ln 2}{\ln n} - 1}T$. For $n > 2$ (which is necessary for cooling to occur in the first place) this implies a negative exponent, ensuring cooling always occurs. From Eq. 18 and Figure 4, we see the work cost is upper bounded by $n^r \bar{w}(T) + n^{r-1} \bar{w}((2/n)T) + \dots + n \bar{w}((2/n)^{r-1}T)$, which in turn is upper bounded by $rn^r \bar{w}(T) = N \ln N \bar{w}(T) / \ln n$. However, because \bar{w} vanishes exponentially with decreasing temperature, only the first few terms in the sum contribute meaningfully, and the work expenditure, therefore, remains of order N . Summing up, this evidences the non-trivial fact that one can, at least in principle, cool down to arbitrarily low temperature at fixed complexity and fixed work cost per qubit. The price to be paid is that of a slower scaling of cooling.

Recent progress of quantum computing technology has exhibited a slow but steady decrease in noise levels, but a relatively fast increase in the total number of qubits. Large numbers of moderately low-noise qubits render the sub-optimal cooling described above a very viable scheme for the near-future. It should be noted, however, that such schemes may require the connectivity of qubits to be re-considered in superconducting qubit implementations, which usually provide lattice-shaped connectivity. Ion-trap quantum computers, which provide all-to-all qubit connectivity, may be better suited for such clustered dynamic cooling.

ACKNOWLEDGMENTS

LBO gratefully acknowledges funding from the European Union's Horizon 2020 research and innovation program under the Marie Skłodowska-Curie grant agreement No 101063316.

Appendix A: Illustrative examples of maximal dynamic cooling

A simple procedure to implement maximal cooling amongst N qubits is as follows: consider listing 2^N all states in increasing lexicographic order, i.e., $|0\dots000\rangle, |0\dots001\rangle, |0\dots010\rangle, |0\dots011\rangle, \dots, |1\dots111\rangle$. The states in the first half of this list all have the target qubit set to 0 ($i_1 = 0$), and thus have the lower eigenenergy of $K, -\hbar\omega/2$. To maximize cooling, we therefore need to construct a unitary U that maps the $\frac{2^N}{2}$ states of ρ with the highest occupation probabilities to the states in the first half of this list. We emphasize that, for the case of cooling a single target qubit, the order of probabilities within the first half of the list does not matter; all that matters is that the half of states with the highest probabilities are mapped to the first half of the lexicographically ordered list. Amongst the degenerate family of unitaries, there is a special transformation, which can be derived with the so-called partner pairing algorithm (PPA), which was demonstrated to be optimal in the entropy manipulation step of (heat bath) algorithmic cooling protocols. The PPA generates a permutation such that states in increasing lexicographic order have non-increasing probabilities. This automatically ensures that the highest probabilities reside in the first half of the lexicographically ordered list. Other special transformations we will examine are the *mirror protocol*, which allows for simple preparation of the cooling unitary, and the *minimal work protocol*, which performs maximal cooling with minimal work cost. These will be explained in more detail through the following illustrative examples with $N = 3$ and $N = 4$ qubits.

1. Maximal cooling with $N = 3$ identical qubits

Consider three identical qubits all initialized at the same temperature T . Our goal is to maximally cool the first qubit below this temperature with the application of a unitary U on all three qubits.

If one lists the $2^N = 8$ states of the total system in lexicographic order, shown in column 2 of Table I, one sees that they are listed in order of increasing eigenenergies of K : the states in the first half of the list, of the form $|0 i_2 i_3\rangle$, have eigenenergy $-\hbar\omega/2$, while the states in the second half of the list, of the form $|1 i_2 i_3\rangle$ have eigenenergy $+\hbar\omega/2$. Initial occupation probabilities of each state p_i are given in column 3, where $x \equiv P_1$ is the initial occupation probability of the excited state for the target qubit. Notice that the $\frac{2^N}{2} = 4$ largest occupation probabilities are not in the first half of the list. Specifically, the 4 highest probabilities are $(1-x)^3, x(1-x)^2, x(1-x)^2, x(1-x^2)$. However, one of these values appears in the lower half of the list. Using the PPA, maximal cooling can be achieved by reordering the probabilities in non-increasing order, which can be accomplished by swapping the two states $|011\rangle$ and $|110\rangle$.

i	$ i\rangle$	p_i	$ \sigma(i)\rangle$	$p_{\sigma(i)}$	$ \sigma_B(i)\rangle$	$p_{\sigma_B(i)}$
0	$ 000\rangle$	$(1-x)^3$	$ 000\rangle$	$(1-x)^3$	$ 001\rangle$	$x(1-x)^2$
1	$ 001\rangle$	$x(1-x)^2$	$ 001\rangle$	$x(1-x)^2$	$ 100\rangle$	$x(1-x)^2$
2	$ 010\rangle$	$x(1-x)^2$	$ 010\rangle$	$x(1-x)^2$	$ 010\rangle$	$x(1-x)^2$
3	$ 011\rangle$	$x^2(1-x)$	$ 100\rangle$	$x(1-x)^2$	$ 000\rangle$	$(1-x)^3$
4	$ 100\rangle$	$x(1-x)^2$	$ 011\rangle$	$x^2(1-x)$	$ 101\rangle$	$x^2(1-x)$
5	$ 101\rangle$	$x^2(1-x)$	$ 101\rangle$	$x^2(1-x)$	$ 111\rangle$	x^3
6	$ 110\rangle$	$x^2(1-x)$	$ 110\rangle$	$x^2(1-x)$	$ 110\rangle$	$x^2(1-x)$
7	$ 111\rangle$	x^3	$ 111\rangle$	x^3	$ 011\rangle$	$x^2(1-x)$

TABLE I. All states of the $N = 3$ qubit system listed in lexicographic order (column 2) with their initial occupation probabilities p_i (column 3). Columns 4 and 6 give various permutations, while columns 5 and 7 give the final occupation probabilities of each state after the respective permutation. (For better readability the states that are not being displaced by the permutation are in grey).

This permutation can be carried out with a unitary operator U , defined in the computation basis, as

To gain a better understanding of how this unitary performs optimal cooling, we examine how the population of the excited state of the target qubit changes before and after this transformation. Recall that P_1 and P'_1 denote the occupation probability of the target qubit's excited state before and after the application of U , respectively. Thus,

$$P_1 = P_{100} + P_{101} + P_{110} + P_{111} \quad (\text{A2})$$

$$P'_1 = P'_{100} + P'_{101} + P'_{110} + P'_{111}, \quad (\text{A3})$$

where $P_{i_1 i_2 i_3}$ is the occupation probability of the state $|i_1 i_2 i_3\rangle$. Now, U implements a transformation that swaps the state $|100\rangle$ with the state $|011\rangle$. Accordingly, it exchanges the populations of the two states, that is $P'_{100} = P_{011}$, and $P'_{011} = P_{100}$, while leaving all other populations unaltered. It follows that

$$\begin{aligned} P'_1 &= P'_{100} + P'_{101} + P'_{110} + P'_{111} \\ &= P_{011} + P_{101} + P_{110} + P_{111} \\ &< P_{100} + P_{101} + P_{110} + P_{111} \\ &= P_1 \end{aligned} \quad (\text{A4})$$

because the probability $P_{011} = e^{-\hbar\omega\beta/2}/Z^3$ featuring two excitations is lower than $P_{100} = e^{\hbar\omega\beta/2}/Z^3$ featuring only one excitation. From Eq. (A4) it follows that

$$P'_1(P_1, 3) = 3P_1^2 - 2P_1^3. \quad (\text{A5})$$

Thus, for $0 < P_1 < 1/2$ (i.e., $T > 0$), we have $P'_1 < P_1$, namely the target qubit is cooled.

Due to the degeneracy in the spectra of ρ and K , there exists a family of degenerate unitaries that can achieve maximal cooling. For example, any unitary of the form in Eq. (A1), but with arbitrary phases replacing the 1's, can also achieve maximal cooling. Furthermore, any unitary that swaps states with equal occupation probabilities (in addition to the swap $|100\rangle \leftrightarrow |011\rangle$) also achieves maximal cooling. In fact, there even exist unitaries performing maximal cooling that implement permutations with cycle lengths greater than two (nb: a swap is a permutation cycle of length two). An example of such a unitary is given by σ_B in column 6 in Table I, featuring the single cycle of length 6 given by $|000\rangle \rightarrow |001\rangle \rightarrow |100\rangle \rightarrow |101\rangle \rightarrow |111\rangle \rightarrow |011\rangle \rightarrow |000\rangle$. In this case, the probabilities are no longer in non-increasing order. However, the 4 largest probabilities reside in the first half of the list, which implies maximal cooling of the target qubit is implemented.

In the case of $N = 3$ qubits, the mirror protocol and the minimal work protocol use the same cooling unitary as the PPA. Therefore, we reserve explanation of these two protocols until the next illustrative example with $N = 4$ qubits, where all three protocols can generate different maximally cooling permutations.

Finally, we remark that cooling cannot be achieved with a total of $N = 2$ identical qubits. If the $2^2 = 4$ states are ordered in increasing lexicographic order, $|00\rangle, |01\rangle, |10\rangle, |11\rangle$, the states are automatically listed in order of increasing eigenenergy of K (i.e., energy of the target qubit), and we see that the two highest probabilities already occupy the first half of the list. Thus, the target qubit cannot be further cooled.

2. Maximal cooling with $N = 4$ identical qubits

We now consider the case of $N = 4$ qubits. As before, we list the $2^N = 16$ states of the total system in increasing lexicographic order, as shown in column 2 of Table II. Again, this automatically orders the states by increasing eigenenergies of K : the states in the first half of the list, of the form $|0 i_2 i_3 i_4\rangle$, have eigenenergy $-\hbar\omega/2$, while the states in the second half of the list, of the form $|1 i_2 i_3 i_4\rangle$, have eigenenergy $+\hbar\omega/2$. The occupation probabilities of the total system states p_i are now denoted by symbols in column 4 of Table II to guide the eye to more quickly recognize patterns, where $\blacksquare \doteq (1-x)^4$; $\blacktriangle \doteq (1-x)^3x$; $\mid \doteq (1-x)^2x^2$; $\bullet \doteq (1-x)x^3$; $_ \doteq x^4$. Again, $x \equiv P_1$ is the initial occupation probability of the excited state for the target qubit. Roughly, the more vertices the symbol has, the higher the probability it represents. The $\frac{2^N}{2} = 8$ largest occupation probabilities can thus be represented by a set containing one \blacksquare , four \blacktriangle 's, and three out of the six \mid 's. The energy of the total system E_i for each state is given in column 3, which is relevant for determining permutations that maximally cool with minimal work cost.

There are a number of permutations that will transform the probabilities in the first half of the list into the 8 largest probabilities, three of which are shown in Table II. The first is a permutation generated according to the PPA σ_{PPA} , which permutes all the probabilities into non-increasing order. Note that there is a degenerate family of permutations that can be generated by the PPA. One such permutation, given in column 5 of Table II, features two cycles of length 2 (i.e. two swaps) given by $|0011\rangle \leftrightarrow |1000\rangle$ and $|0111\rangle \leftrightarrow |1100\rangle$.

The second permutation, σ_W , given in column 7 of Table II, features one of a degenerate family of minimal work protocols, which achieves maximal cooling with minimal work cost. In short, after the maximal cooling is achieved by moving the highest half of probabilities to the top half of the list, the minimal work protocol sorts the probabilities within each half of the list

i	$ i\rangle$	$E_i[\hbar\omega/2]$	p_i	$ \sigma_{PPA}(i)\rangle$	$p_{\sigma_{PPA}(i)}$	$ \sigma_W(i)\rangle$	$p_{\sigma_W(i)}$	$ \sigma_M(i)\rangle$	$p_{\sigma_M(i)}$
0	$ 0000\rangle$	-4	■	$ 0000\rangle$	■	$ 0000\rangle$	■	$ 0000\rangle$	■
1	$ 0001\rangle$	-2	▲	$ 0001\rangle$	▲	$ 0001\rangle$	▲	$ 0001\rangle$	▲
2	$ 0010\rangle$	-2	▲	$ 0010\rangle$	▲	$ 0010\rangle$	▲	$ 0010\rangle$	▲
3	$ 0011\rangle$	0		$ 1000\rangle$	▲	$ 0011\rangle$		$ 0011\rangle$	
4	$ 0100\rangle$	-2	▲	$ 0100\rangle$	▲	$ 0100\rangle$	▲	$ 0100\rangle$	▲
5	$ 0101\rangle$	0		$ 0101\rangle$		$ 0101\rangle$		$ 0101\rangle$	
6	$ 0110\rangle$	0		$ 0110\rangle$		$ 1000\rangle$	▲	$ 0110\rangle$	
7	$ 0111\rangle$	2	•	$ 1100\rangle$		$ 1010\rangle$		$ 1000\rangle$	▲
8	$ 1000\rangle$	-2	▲	$ 0011\rangle$		$ 0110\rangle$		$ 0111\rangle$	•
9	$ 1001\rangle$	0		$ 1001\rangle$		$ 1001\rangle$		$ 1001\rangle$	
10	$ 1010\rangle$	0		$ 1010\rangle$		$ 0111\rangle$	•	$ 1010\rangle$	
11	$ 1011\rangle$	2	•	$ 1011\rangle$	•	$ 1011\rangle$	•	$ 1011\rangle$	•
12	$ 1100\rangle$	0		$ 0111\rangle$	•	$ 1100\rangle$		$ 1100\rangle$	
13	$ 1101\rangle$	2	•	$ 1101\rangle$	•	$ 1101\rangle$	•	$ 1101\rangle$	•
14	$ 1110\rangle$	2	•	$ 1110\rangle$	•	$ 1110\rangle$	•	$ 1110\rangle$	•
15	$ 1111\rangle$	4	—	$ 1111\rangle$	—	$ 1111\rangle$	—	$ 1111\rangle$	—

TABLE II. All states of the $N = 4$ qubit system listed in lexicographic order (column 2) with total state energy (column 3) and their initial occupation probabilities (column 4). Columns 5, 7, and 9 give various permutations, while columns 6, 8, and 10 give the final occupation probabilities of each state after the respective permutation. Occupation probabilities are represented by symbols, where ■ $\doteq (1-x)^4$; ▲ $\doteq (1-x)^3x$; | $\doteq (1-x)^2x^2$; • $\doteq (1-x)x^3$; — $\doteq x^4$. (For better readability the states that are not being displaced by the permutation are in grey).

separately. Within each half-list, the highest probability is assigned to the state with the lowest total system energy, the second highest probability is assigned to the state with the second lowest total system energy, etc. It turns out that in the case of $N = 4$ qubits, the PPA also belongs to the family of minimal work protocols, but this is not generally the case.

The third permutation, σ_M , given in column 9 of Table II, enacts what we call the *mirror* protocol. In the mirror protocol, states that have the target qubit set to 0 and have a total of $k < N/2$ bits set to 0 are swapped with their mirror image (also, called the negative image). The idea is that these are the states in the top half of the lexicographically ordered list that have lower probabilities than their mirror-image state in the bottom half of the list. This is because a state with $k < N/2$ bits set to zero will necessarily have fewer bits set to zero than its mirror image, and thereby have a lower occupation probability. These mirror-image swaps ensure that all states with the target qubit set to 0 are assigned a higher probability than their mirror-image state, which necessarily have the target qubit set to 1. In turn, this means the highest half of probabilities will reside in the first half of the lexicographically ordered list. The advantage of the mirror protocol is two-fold: (i) the ease with which one can automatically generate the maximally cooling unitary for any system size N and (ii) the protocol generates a single, unique cooling unitary for each system size N , as opposed to the PPA and minimum work protocols which can generate a family of degenerate cooling unitaries.

In the mirror protocol for the case of $N = 4$, we seek states that start with 0 and have $k < N/2 = 2$ total bits set to 0. The only state that adheres to these criteria is the state $|0111\rangle$, which we swap with its mirror image: $|1000\rangle$. Notice that it is not a minimal work protocol as the state in the first half of the list with highest total energy $|0111\rangle$ is not assigned the lowest probability in the top-half of the list. Note, also, that the permutation σ on $N = 3$ qubits, given in Table I is an instance of the mirror protocol, as well as a minimal work protocol.

To convince ourselves that all three permutations in Table II all perform maximal cooling, we can compute the probability of the excited state of the target qubit P'_1 after each transformation. In this case, $P'_1 = P'_{1000} + P'_{1001} + P'_{1010} + P'_{1011} + P'_{1100} + P'_{1101} + P'_{1110} + P'_{1111}$. By consulting what these constituent probabilities are after each permutation in Table II, one finds that in all cases:

$$P'_1(P_1, 4) = 3P_1^2 - 2P_1^3. \quad (\text{A6})$$

This is exactly the same expression found for the $N = 3$ case. Namely, adding a fourth qubit did not increase the cooling power. This is a special case of a more general result: There is no cooling gain in going from an odd N to $N + 1$. Adding a fourth qubit, however, has the adverse effect of increasing the complexity of the unitary operation needed to implement the cooling (in general, operators acting on larger Hilbert spaces are more complex). In fact, for a given system size N , different permutations will carry different complexities in terms of their implementation in quantum circuits. Notice that the permutation σ_M in Table II contains one permutation cycle of length 2 (i.e., a swap) which acts on all the qubits, while σ_W contains two swaps, but each swap only acts on three out of the four qubits. Such characteristics of the permutation will alter the complexity of the final

quantum circuit, and should therefore be considered from a practical standpoint when implementing such cooling algorithms on quantum computers.

Another crucial point is that distinct permutations that achieve maximal cooling are generally accompanied by distinct energy costs. For example, the work accompanying the permutation σ_M (see equation 16 in the main text) is:

$$\begin{aligned} W_{\sigma_M} &= (\hbar\omega/2)[2(\Delta - \bullet) + (-2)(\bullet - \Delta)] \\ &= 2\hbar\omega[P_0^3 P_1 - P_0 P_1^3]. \end{aligned} \quad (\text{A7})$$

Similarly, the work accompanying the permutation σ_W is

$$\begin{aligned} W_{\sigma_W} &= (\hbar\omega/2)[2(| - \bullet) + (-2)(| - \Delta)] \\ &= \hbar\omega[(P_0)^3 P_1 - P_0 P_1^3]. \end{aligned} \quad (\text{A8})$$

Note that the minimal work permutation costs half work of the mirror protocol. σ_W is more energy efficient than σ_M while achieving the same cooling power $P'_1(P_1, 4)$. Hence σ_W may be preferable when it comes to practical applications.

Appendix B: Proof that $P'_1(P_1, 2s - 1) = P'_1(P_1, 2s)$

Below is the proof that, in general $P'_1(P_1, 2s - 1) = P'_1(P_1, 2s)$ for $s \in \mathbb{N}$. For ease of notation we set $x \equiv P_1$ and $y \equiv P'_1$. Note that in this notation, $(1 - x) \equiv P_0$. For $N = 2s$, we have

$$\begin{aligned} y(x, N) &= \sum_{0 \leq k \leq \frac{N}{2}-1} \binom{N}{k} (1-x)^k x^{N-k} + \frac{1}{2} \binom{N}{\frac{N}{2}} (1-x)^{\frac{N}{2}} x^{\frac{N}{2}} \\ &= \binom{N}{0} x^N + \sum_{1 \leq k \leq \frac{N}{2}-1} \left[\binom{N-1}{k} + \binom{N-1}{k-1} \right] (1-x)^k x^{N-k} + \frac{1}{2} \binom{N}{\frac{N}{2}} (1-x)^{\frac{N}{2}} x^{\frac{N}{2}} \\ &= x \left[\binom{N}{0} x^{N-1} + \sum_{1 \leq k \leq \frac{N}{2}-1} \binom{N-1}{k} (1-x)^k x^{N-k-1} \right] + \sum_{1 \leq k \leq \frac{N}{2}-1} \binom{N-1}{k-1} (1-x)^k x^{N-k} + \frac{1}{2} \binom{N}{\frac{N}{2}} (1-x)^{\frac{N}{2}} x^{\frac{N}{2}} \\ &= xy(x, N-1) + (1-x) \left[\sum_{0 \leq q \leq \frac{N}{2}-1} \binom{N-1}{q} (1-x)^q x^{N-1-q} + \frac{1}{2} \left[\binom{N-1}{\frac{N}{2}-1} + \binom{N-1}{\frac{N}{2}} \right] (1-x)^{\frac{N-2}{2}} x^{\frac{N}{2}} \right] \\ &= xy(x, N-1) + (1-x) \left[\sum_{0 \leq q \leq \frac{N}{2}-1} \binom{N-1}{q} (1-x)^q x^{N-1-q} + \binom{N-1}{\frac{N}{2}-1} (1-x)^{\frac{N}{2}-1} x^{\frac{N}{2}} \right] \\ &= xy(x, N-1) + (1-x) \left[\sum_{0 \leq q \leq \frac{N}{2}} \binom{N-1}{q} (1-x)^q x^{N-1-q} \right] \\ &= xy(x, N-1) + (1-x)y(x, N-1) \\ &= y(x, N-1). \end{aligned} \quad (\text{B1})$$

In the second line we used the identity $\binom{N}{k} = \binom{N-1}{k} + \binom{N-1}{k-1}$. In the fourth line we used a change of variable $q = k - 1$. In the sixth line we used the fact that $\binom{N-1}{\frac{N}{2}-1} = \binom{N-1}{\frac{N}{2}}$ for even N .

Appendix C: Derivation of $c_s \simeq (2/\sqrt{\pi})\sqrt{s}$

We have:

$$\begin{aligned} &\sum_{k=0}^{s-1} \binom{2s-1}{k} (2s-1-2k) \\ &= (2s-1) \sum_{k=0}^{s-1} \binom{2s-1}{k} - 2 \sum_{k=0}^{s-1} k \binom{2s-1}{k} \end{aligned} \quad (\text{C1})$$

Using the identity

$$\sum_{k=0}^n \binom{n}{k} = 2^n \quad (\text{C2})$$

we obtain:

$$\sum_{k=0}^{s-1} \binom{2s-1}{k} = \frac{1}{2} \sum_{k=0}^{2s-1} \binom{2s-1}{k} = \frac{1}{2} 2^{2s-1} = 2^{2s-2} \quad (\text{C3})$$

where we used the fact that the binomial coefficient is symmetric with respect to reflection about its point of maximum.

Using the identity

$$k \binom{n}{k} = n \binom{n-1}{k-1} \quad (\text{C4})$$

we get

$$\begin{aligned} \sum_{k=0}^{s-1} k \binom{2s-1}{k} &= \sum_{k=1}^{s-1} k \binom{2s-1}{k} \\ &= (2s-1) \sum_{k=1}^{s-1} \binom{2s-2}{k-1} \end{aligned} \quad (\text{C5})$$

Furthermore

$$2^{2s-2} = \sum_{k=0}^{2s-2} \binom{2s-2}{k} = 2 \sum_{k=0}^{s-2} \binom{2s-2}{k} + \binom{2s-2}{s-1} \quad (\text{C6})$$

where we used the reflection symmetry of the binomial coefficient and kept in mind not to count the mid value $\binom{2s-2}{s-1}$ twice. From the above equation it follows that:

$$\sum_{k=1}^{s-1} \binom{2s-2}{k-1} = \sum_{k=0}^{s-2} \binom{2s-2}{k} = \frac{1}{2} \left(2^{2s-2} - \binom{2s-2}{s-1} \right) \quad (\text{C7})$$

Summing up:

$$\begin{aligned} &\sum_{k=0}^{s-1} \binom{2s-1}{k} (2s-1-2k) \\ &= (2s-1) 2^{2s-2} - (2s-1) \left(2^{2s-2} - \binom{2s-2}{s-1} \right) \\ &= (2s-1) \binom{2s-2}{s-1} \\ &= s \binom{2s-1}{s} \end{aligned} \quad (\text{C8})$$

where we use Eq. (C4) in the last equality. Therefore:

$$\begin{aligned} c_s &= 2^{2-2s} \sum_{k=0}^{s-1} \binom{2s-1}{k} (2s-1-2k) \\ &= 2^{2-2s} s \binom{2s-1}{s} \\ &= 2^{2-2s} s a_s \end{aligned} \quad (\text{C9})$$

where we used $a_s = \binom{2s-1}{s}$. Using Eq. (D2) we get:

$$\begin{aligned}\ln c_s &\simeq 2 \ln 2 - 2s \ln 2 + \ln s - \ln 2 - \ln \sqrt{\pi} - \ln \sqrt{s} + s \ln 4 \\ &= \ln 2 - \ln \sqrt{\pi} + \ln \sqrt{s}\end{aligned}\quad (\text{C10})$$

and therefore

$$c_s \simeq \frac{2}{\sqrt{\pi}} \sqrt{s}. \quad (\text{C11})$$

Appendix D: Derivation of $a_s \simeq s \ln 4 + O(\ln s)$

Using Stirling's approximation

$$N! \simeq \sqrt{2\pi N} (N/e)^N \quad (\text{D1})$$

one finds

$$\begin{aligned}\ln a_s = \ln \binom{2s-1}{s} &\simeq \frac{1}{2} \ln(2\pi) + \frac{1}{2} \ln(2s-1) + (2s-1) \ln(2s-1) - (2s-1) \\ &\quad - \frac{1}{2} \ln(2\pi) - \frac{1}{2} \ln s - s \ln s + s \\ &\quad - \frac{1}{2} \ln(2\pi) - \frac{1}{2} \ln(s-1) - (s-1) \ln(s-1) + s - 1 \\ &\simeq -\ln(2\pi) - \frac{1}{2} \ln s + s \ln 4\end{aligned}\quad (\text{D2})$$

that is $a_s \simeq s \ln 4 + O(\ln s)$ where $O(\ln s)$ stands for terms that scale at most like $\ln s$.

Appendix E: Illustrative example of quantum circuit construction

We demonstrate the generation of the sub-circuit for permutation between the two states $|01111\rangle$ and $|10000\rangle$. To implement the sub-circuit for this swap we let $b_1 = 01111$ and $b_2 = 10000$ and define a Gray code from b_1 to b_2 , such as the following:

$$\begin{array}{c} 01111 \\ 11111 \\ 10111 \\ 10011 \\ 10001 \\ 10000. \end{array} \quad (\text{E1})$$

Here, the length of the Gray code is $m = 6$. To construct the circuit for the swap, we insert one $C^k(X)$ gate to transform between successive states in the Gray code. After insertion of $m - 1$ $C^k(X)$ gates, the circuit will successfully transform an input state b_1 to b_2 . To implement the reverse transformation (since we wish to swap the two states), and uncompute any changes made to other input states not involved in the swap, it is necessary to add the first $m - 2$ $C^k(X)$ gates in reverse order. Thus, a quantum circuit implementing a swap between states with a Gray code of length m will contain $2m - 3$ $C^k(X)$ gates. The quantum circuit implementing the swap between b_1 and b_2 using the Gray code in equation E1 is depicted in Figure 7.

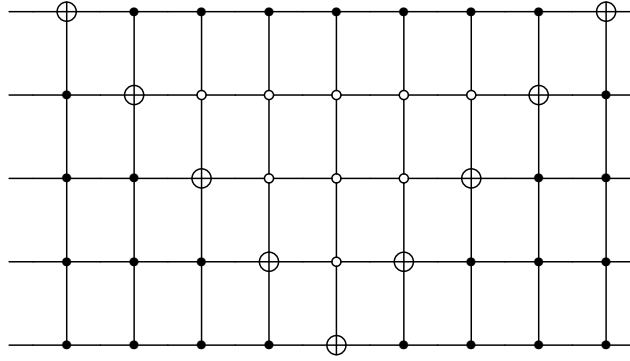


FIG. 7. Quantum circuit implementing a swap between states $|01111\rangle$ and $|10000\rangle$ using the Gray code shown in equation E1. Each wire represents a qubit in system. The circuit is comprised of $2m - 3 C^k(X)$ gates, where $m = 6$ is the length of the Gray code and $N = 5$ is the number of qubits in the system. Open circles with a cross in the $C^k(X)$ gates are the NOT (i.e., Pauli-X) gate, closed circles imply the NOT gate is applied when the corresponding control qubit is in the $|1\rangle$ state, while open circles imply the NOT gate is applied when the corresponding control qubit is in the $|0\rangle$ state.

[1] J. Preskill, Reliable quantum computers, *Proceedings of the Royal Society of London. Series A: Mathematical, Physical and Engineering Sciences* **454**, 385 (1998).

[2] L. Bassman, M. Urbanek, M. Metcalf, J. Carter, A. F. Kemper, and W. A. de Jong, Simulating quantum materials with digital quantum computers, *Quantum Science and Technology* **6**, 043002 (2021).

[3] D. P. DiVincenzo, The physical implementation of quantum computation, *Fortschritte der Physik: Progress of Physics* **48**, 771 (2000).

[4] E. Knill, R. Laflamme, and W. H. Zurek, Resilient quantum computation, *Science* **279**, 342 (1998).

[5] D. Aharonov and M. Ben-Or, Fault-tolerant quantum computation with constant error, in *Proceedings of the twenty-ninth annual ACM symposium on Theory of computing* (1997) pp. 176–188.

[6] G. A. Morris and R. Freeman, Enhancement of nuclear magnetic resonance signals by polarization transfer, *Journal of the American Chemical Society* **101**, 760 (1979).

[7] O. W. Sørensen, Polarization transfer experiments in high-resolution nmr spectroscopy, *Progress in nuclear magnetic resonance spectroscopy* **21**, 503 (1989).

[8] L. J. Schulman and U. Vazirani, Scalable nmr quantum computation, *arXiv preprint quant-ph/9804060* (1998).

[9] L. J. Schulman and U. V. Vazirani, Molecular scale heat engines and scalable quantum computation, in *Proceedings of the thirty-first annual ACM symposium on Theory of computing* (1999) pp. 322–329.

[10] A. E. Allahverdyan, K. V. Hovhannyan, D. Janzing, and G. Mahler, Thermodynamic limits of dynamic cooling, *Physical Review E* **84**, 041109 (2011).

[11] P. O. Boykin, T. Mor, V. Roychowdhury, F. Vatan, and R. Vrijen, Algorithmic cooling and scalable nmr quantum computers, *Proceedings of the National Academy of Sciences* **99**, 3388 (2002).

[12] J. M. Fernandez, S. Lloyd, T. Mor, and V. Roychowdhury, Algorithmic cooling of spins: A practicable method for increasing polarization, *International Journal of Quantum Information* **2**, 461 (2004).

[13] L. J. Schulman, T. Mor, and Y. Weinstein, Physical limits of heat-bath algorithmic cooling, *Physical review letters* **94**, 120501 (2005).

[14] J. M. Fernandez, T. Mor, and Y. Weinstein, Paramagnetic materials and practical algorithmic cooling for nmr quantum computing, *International Journal of Quantum Information* **3**, 281 (2005).

[15] J. Baugh, O. Moussa, C. A. Ryan, A. Nayak, and R. Laflamme, Experimental implementation of heat-bath algorithmic cooling using solid-state nuclear magnetic resonance, *Nature* **438**, 470 (2005).

[16] F. Rempp, M. Michel, and G. Mahler, Cyclic cooling algorithm, *Physical Review A* **76**, 032325 (2007).

[17] P. Kaye, Cooling algorithms based on the 3-bit majority, *Quantum Information Processing* **6**, 295 (2007).

[18] C. Ryan, O. Moussa, J. Baugh, and R. Laflamme, Spin based heat engine: demonstration of multiple rounds of algorithmic cooling, *Physical review letters* **100**, 140501 (2008).

[19] Y. Elias, T. Mor, and Y. Weinstein, Semioptimal practicable algorithmic cooling, *Physical Review A* **83**, 042340 (2011).

[20] F. Ticozzi and L. Viola, Quantum resources for purification and cooling: fundamental limits and opportunities, *Scientific reports* **4**, 5192 (2014).

[21] G. Brassard, Y. Elias, T. Mor, and Y. Weinstein, Prospects and limitations of algorithmic cooling, *The European Physical Journal Plus* **129**, 1 (2014).

[22] G. Brassard, Y. Elias, J. M. Fernandez, H. Gilboa, J. A. Jones, T. Mor, Y. Weinstein, and L. Xiao, Experimental heat-bath cooling of spins, *The European Physical Journal Plus* **129**, 1 (2014).

[23] S. Raeisi and M. Mosca, Asymptotic bound for heat-bath algorithmic cooling, *Physical review letters* **114**, 100404 (2015).

[24] N. A. Rodríguez-Briones and R. Laflamme, Achievable polarization for heat-bath algorithmic cooling, *Physical review letters* **116**, 170501 (2016).

[25] Y. Atia, Y. Elias, T. Mor, and Y. Weinstein, Algorithmic cooling in liquid-state nuclear magnetic resonance, *Physical Review A* **93**, 012325 (2016).

- [26] N. A. Rodríguez-Briones, E. Martín-Martínez, A. Kempf, and R. Laflamme, Correlation-enhanced algorithmic cooling, *Physical review letters* **119**, 050502 (2017).
- [27] S. Racisi, M. Kieferová, and M. Mosca, Novel technique for robust optimal algorithmic cooling, *Physical review letters* **122**, 220501 (2019).
- [28] F. Arute, K. Arya, R. Babbush, D. Bacon, J. C. Bardin, R. Barends, R. Biswas, S. Boixo, F. G. Brandao, D. A. Buell, *et al.*, Quantum supremacy using a programmable superconducting processor, *Nature* **574**, 505 (2019).
- [29] C. D. Bruzewicz, J. Chiaverini, R. McConnell, and J. M. Sage, Trapped-ion quantum computing: Progress and challenges, *Applied Physics Reviews* **6** (2019).
- [30] A. Auffèves, Quantum technologies need a quantum energy initiative, *PRX Quantum* **3**, 020101 (2022).
- [31] A. E. Allahverdyan, R. Balian, and T. M. Nieuwenhuizen, Maximal work extraction from finite quantum systems, *Europhysics Letters* **67**, 565 (2004).
- [32] A. Solfanelli, A. Santini, and M. Campisi, Quantum thermodynamic methods to purify a qubit on a quantum processing unit, *AVS Quantum Science* **4**, 026802 (2022).
- [33] M. A. Nielsen and I. Chuang, *Quantum computation and quantum information* (2002).
- [34] A. Barenco, C. H. Bennett, R. Cleve, D. P. DiVincenzo, N. Margolus, P. Shor, T. Sleator, J. A. Smolin, and H. Weinfurter, Elementary gates for quantum computation, *Physical review A* **52**, 3457 (1995).
- [35] K. Temme, S. Bravyi, and J. M. Gambetta, Error mitigation for short-depth quantum circuits, *Physical review letters* **119**, 180509 (2017).
- [36] M. Urbanek, B. Nachman, V. R. Pascuzzi, A. He, C. W. Bauer, and W. A. de Jong, Mitigating depolarizing noise on quantum computers with noise-estimation circuits, *Physical Review Letters* **127**, 270502 (2021).
- [37] M. Dupont and J. E. Moore, Quantum criticality using a superconducting quantum processor, *Physical Review B* **106**, L041109 (2022).
- [38] L. B. Oftelie, R. Van Beeumen, D. Camps, W. A. de Jong, and M. Dupont, Simulating dirty bosons on a quantum computer, *New Journal of Physics* (2024).